Check for updates

Asymmetric L-shaped resonant optical antennas with plasmon length tuning and high-electric field enhancement

Nikola Bralović[1] · Uli Lemmer[1,2] · Mohamed Hussein[1,3]

Abstract

L-shaped resonant optical antennas (ROAs) are low-symmetry plasmonic nanostructures with the unique ability to show two tunable resonances in the optical and near-infrared wavelength regions. The plasmon length of the so-called longitudinal dipolar fundamental plasmon mode of these asymmetric L-shaped ROAs can be used as plasmon resonance building blocks to design polarization-sensitive devices. This paper introduces and numerically analyzes a novel design of asymmetric L-shape ROAs. The reported design offers two resonance modes, i.e., bimodal longitudinal antenna resonance behavior with a high enhancement factor. These two resonances can be selectively excited by changing the linear polarization angle. It is found that the coupled L-shaped ROA with a very small 2 nm gap width exhibits field enhancements 40 and 147.3 on scale $\left|E_{TOT}\right|/\left|E_{IN}\right|$ for the high energy and low energy resonance, respectively. The obtained results and the analysis open a new route for multiple plasmon resonance devices with ultra-high field enhancement that can be easily integrated with future nano-optical circuits with multiple operational frequencies.

Keywords Resonant optical antenna · Plasmonic structures · COMSOL · Field enhancement

✉ Uli Lemmer
   ulrich.lemmer@kit.edu

✉ Mohamed Hussein
   mohamed.hussein@kit.edu

1   Light Technology Institute (LTI), Karlsruhe Institute of Technology (KIT), Kaiserstraße 12, 76131 Karlsruhe, Germany

2   Institute of Microstructure Technology (IMT), Karlsruhe Institute of Technology (KIT), Hermann-Von-Helmholtz-Platz 1, 76344 Eggenstein-Leopoldshafen, Germany

3   Department of Physics, Faculty of Science, Ain Shams University, Abbassia 11566, Cairo, Egypt

1 Introduction

In the last couple of years, there is a growing interest in the field of light-matter interaction with novel applications of the electromagnetic properties of nanoscale metals, such as resonant optical antennas (Mühlschlegel et al. 2005; Bharadwaj et al. 2009; Novotny and van Hulst 2011; Biagioni et al. 2012; Kern et al. 2015; Curto et al. 2010; Feichtner et al. 2017; Giannini et al. 2011) and metamaterials (Veselago 1968). Due to the collective oscillations of the free carriers confined to the metal particle volume or so-called localized surface plasmon resonances, noble metal nanoparticles are prominent for their volume-dependent scattering and absorption properties that furthermore can be tuned throughout the visible and NIR wavelength range by shaping their specific geometry, their materials composition properties and their environment (Kelly et al. 2008). As a result, the optical response function in the vis/NIR-wavelength region and the locally enhanced fields can be tuned according to the application needs. Therefore, resonance design toolbox parameter so-called plasmon length is introduced. It can be described as the length scale over which the free electron oscillation takes place (Ringe et al. 2012). Highly localized near-fields at certain frequencies together with specific light polarization conditions are essential for new nonlinear optical effects, such as nonlinear plasmonics via four-wave mixings (Palomba and Novotny 2008) or the increasing sensitivity and selectivity demands for surface-enhanced Raman micro-spectroscopy down to the single molecule limit (Kneipp et al. 1997).

In the field of resonant optical antennas (ROAs) (Mühlschlegel et al. 2005), the scaling laws for their antenna resonance frequency have been motivated by the RF-antenna community design and tools (Novotny 2007). V-shaped ROAs (Zhag and Yang et al., 2007),"bowtie" ROAs (Fromm et al. 2004), and Yagi-Uda ROAs (Kosako et al. 2010) have been investigated numerically. Expanding the ROA architecture towards L-shaped configurations opens pathways for polarization-sensitive plasmon resonance frequencies with fundamental dipolar mode together with the so-called three-pole resonance, which originates from the symmetric current mode running along the antenna arm of the asymmetric L-shape. Symmetric L-shaped nanostructures as ROAs have been extensively studied and proposed (Yang and Zhang 2011, 2013; Jing et al. 2009; Seo et al. 2010; Bai et al. 2015; Tahir et al. 2017; Miao et al. 2022). Also, it had been investigated coupling of L-shaped nanodimers (Black et al., 2015) as a part of efficiency investigation of second harmonic generation over the transition from capacitive to conductive coupling. Furthermore, different polarization conditions for symmetric L-shaped structures are studied (Wang et al. 2015) in order to design ultra-thin optical vortex phase plate (VPP) which can generate the optical vortex beams with different topological charges. Finally, L-shaped slot antennas are explored and used as a nano-router (Xu et al. 2021). In contrast, the literature lacks numerical studies on the performance of asymmetric L-shape designs.

We introduce two novel designs of ROAs based on asymmetric L-shapes with plasmon length tuning and high-electric field enhancement. The performance of the reported design is numerically investigated via finite element method. The suggested ROAs offer two resonances or a bimodal longitudinal antenna resonance behavior. These two resonances' excitations can be controlled by changing the linear polarization angle. The asymmetric L-shaped single ROAs resonances can be interpreted conceptually as tuning the plasmon length accordingly by "fusing" rod-like single particles. This analysis opens a design route for multiple plasmon resonances that match the conditions for future nano-optical active circuits. Table 1 summarizes the current study with the previous work.

Table 1 Comparison of current study with similar structures

Reference	Structure	No of peaks	EF factor
Khalil et al. (2021)	Triple layer structured	3	35,5,82
Li et al. (2012)	Plasmonic staircase nanoantenna	1	32
Sederberg and Elezzabi (2011)	Sierpi´nski fractal plasmonic bowtie	2	7,43
Sederberg and Elezzabi (2011)	Triangular counter bowtie	1	37
Yue et al. (2017)	Triangular bowtie antenna	1	34
Yue et al. (2017)	Dimer	1	12
	This work	2	40,147.3

The paper is organized as follows. Section 2 presents the simulated structures and explains the strategy to identify the plasmon length for size-evolving asymmetric L-shaped ROAs. Section 3 interprets those findings with plasmon length tuning as tools for multiple plasmon resonance ROAs and the detailed simulation results for the reported designs. Finally, conclusions will be drawn in Sect. 4.

2 Geometric parameters and simulation strategy

Figure 1 shows the reported asymmetric L-shaped nanoantennas design in top and 3D views. In this study, the height (H) and the width (W) are kept constant at 30 nm and 20 nm, respectively. All antennas can be fabricated by lithographic techniques reported in (Wissert et al. 2009; Dopf et al. 2015; Schwab et al. 2013). The nanoantenna arm length varies from 20 to 80 nm in steps of 20 nm. All simulation studies are carried out using the Finite Element Method (FEM) (Zienkiewicz et al. 2005) via the commercial software package COMSOL Multiphysics Software (https://www.comsol.com). A maximum mesh element size of 6 nm is used for the L-shaped ROAs which are comprised of rod like antenna arms as rectangular geometric blocks with rounded corners to avoid electromagnetic field singularities. In the remaining area surrounding the nanostructure, the maximum mesh element size is 80 nm. The dielectric constants for gold are taken from (Johnson and
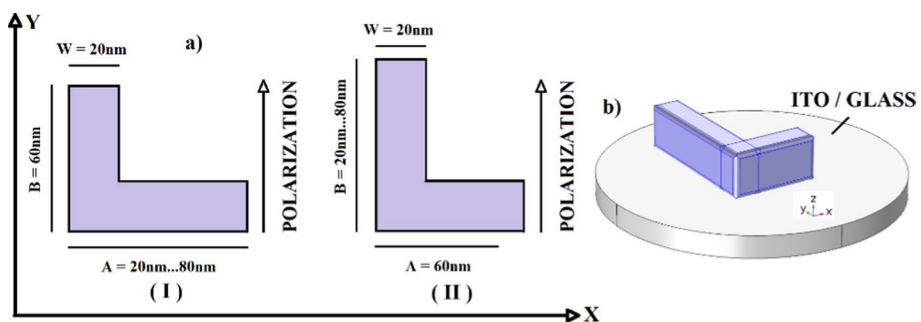

Fig. 1 a Top view of a single L-shaped ROA (x–y plane) with the antenna arms termed A and B in two configuration (I, II) with respect to the linearly polarized plane wave excitation; **b** 3D scheme of gold L-shaped ROA on glass

Christy 1972). The simulation domain has a spherical shape with a radius of 600 nm. All ROA models are surrounded by a sufficient number of perfectly matched layers (PMLs) in x, y and z directions. The numerical models include the ROA supporting layers, such as glass and 50 nm thick ITO (indium tin oxide). The optical response such as the absolute scattering and absorption cross-section as a function of varying arm length is calculated in the wavelength range from 500 to 1000 nm. Furthermore, the 3-D Maxwell solution of our model gives the quantities of the current distribution with its vector representation over the entire volume of the ROA as a function of wavelength. The designed nanoantennas are illuminated by an electromagnetic plane wave propagating from the substrate side with linear polarization properties as indicated in the following. In all simulation results in this paper absorption and scattering cross sections are calculated according to classical antenna theory (Balanis, C.A., 2005).

3   Results and Discussion

a.   L-shape results

The analysis started with the two principal configurations as indicated in Fig. 1a). The asymmetric L-shaped ROA arms are co-aligned (lengths here termed: A, B) with the Cartesian coordinate axes (x,y). The linear excitation polarization of the electromagnetic plane wave is set parallel to the y-axis. For each wavelength, as is indicated above, one of the ROA arm's lengths is increased from 20 nm up to 80 nm individually in steps of 20 nm while the corresponding other ROA arm is held constant at 60 nm. By this method, we generate a set of four ROAs with two orthogonal configurations of rod-like antennas (here termed: I, ROA starting geometry being parallel to the linearly polarized wave and II, ROA starting geometry being perpendicular to the linearly polarized wave) with respect to the linearly polarized plane wave excitation. Thus, the typical antenna parameter L/λ (arm length/wavelength) is evolved as a figure-of-merit not only to derive the ROA resonance scaling, but also to investigate the associated ROA current mode development. Having simulated numerically the far field optical properties of asymmetric L-shaped ROAs, the ROA configuration **I** as indicated in Fig. 1 is analyzed first.

A = 20 nm corresponds to a pure nanorod like ROA. It can be noted that a monomodal longitudinal ROA antenna mode in the absorption as well as in the scattering spectra that originates from the ROA with B = 60 nm. The particle plasmon resonance property of a gold nanorod with an aspect ratio $B/A = 3$ agrees with the previous results already published (Bohren and Huffman 1983). This particular ROA geometry with its associated particle plasmon resonance is an excellent example for the relevance of the plasmon length. The longitudinal current mode here shows that its oscillation is pinned to the physical dimension with well-defined nodes at the nanorod's ends. Increasing the ROAs arm length A and thus breaking the nanorod symmetry leads to the development of bimodal ROA resonance behavior (Fig. 2). When we increase just the length of one ROA arm, we therefore observe two new ROA resonances that shift both to the low energy side of the spectral bandwidth shown here, but with increasing wavelength separation between the bimodal resonance wavelengths. We now switch to the simulation of the abovementioned ROA configuration **II**. For the rod-like ROA (B = 20 nm), a resonance peak in the absorption spectrum at 540 nm is observed that can be interpreted as the transversal particle plasmon resonance which is supported by the vector representation of the volume current mode. It is worth mentioning that, by lowering the symmetry of the rod-like ROA while increasing
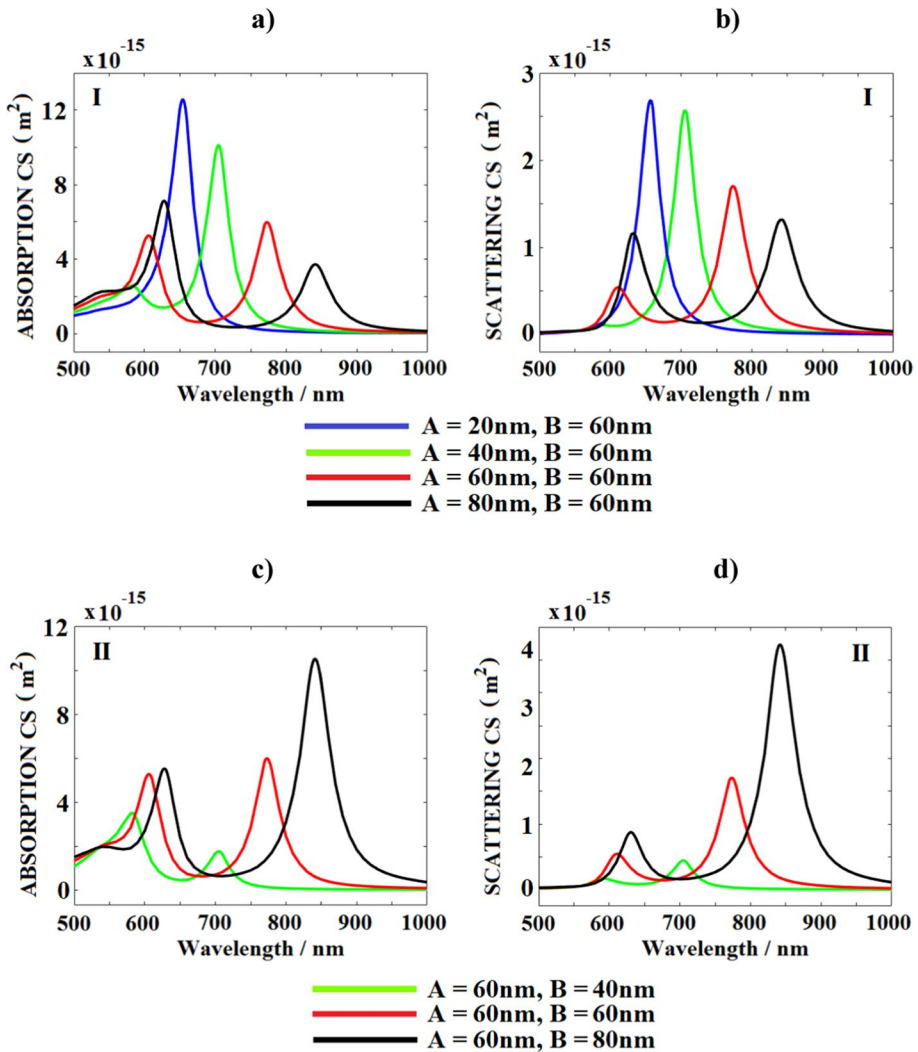
Fig. 2 Far field optical properties of single L-shaped ROAs with increasing arm length, respectively. **a** absolute absorption cross section of ROA for configuration I from Fig. 1a; **b** absolute scattering cross section of ROA for configuration I from Fig. 1a; **c** absolute absorption cross section of ROA for configuration II from Fig. 1a; **d** absolute scattering cross section of ROA for configuration II from Fig. 1a

just the antenna arm length B from 20 to 80 nm, we observe a bimodal ROA resonance property for both the absorption and the scattering spectra that develops its frequency shifting and increasing wavelength separation between the two ROA resonances similar to the case of ROA **I**.

The interesting point here is that this development starts with a transversal particle plasmon mode, and from symmetry considerations concerning the ROA above configuration **I**. It develops into two longitudinal ROA modes with a high-frequency resonance component and a low-frequency resonance counterpart. This analysis is supported by the current mode

representation of the asymmetric L-shaped ROAs depicted in Fig. 3 which shows the current density of the bimodal ROA resonances for the two configurations I and II at the two wavelengths of λ = 634 nm and λ = 843 nm, respectively.

It can be seen from this Fig. that for both configurations **I** and **II**, two distinct modes linked to the bimodal resonances of the L-shaped ROA are evident from the vector representations of the current densities. The signatures of both configurations **I** and **II** have the same qualitative current mode pattern. The low-frequency ROA (eigen mode) can be assigned to a slightly perturbed – bent – longitudinal current mode-giving rise to the ROA resonance at 843 nm, whereas the high-frequency ROA resonance at 634 nm has a current mode signature of an out-of-phase longitudinal resonance oscillating along each individual ROA antenna arm A and B. It is interesting to note that despite the polarization mismatch of the asymmetric L-shaped ROA concerning the linearly polarized excitation plane wave, the highest current density amplitude is exclusively located at the shorter ROA arm of the L-shaped antenna giving rise to the 634 nm ROA resonance.

More insight into the ROA performance is gained from analyzing their specific polarization dependence as a function of frequency. Figure 4 illustrates the variation of the absorption and scattering cross sections with the incident wave polarization. It can be seen from this figure that the optical far-field response function (absorption cross section and the scattering cross section) can be finely tuned by varying the polarization angle to be maximized on the high-frequency ROA resonance or the low-frequency ROA resonance. The asymmetric L-shaped ROA shows a bimodal wavelength-dependent polarization property. As depicted in Fig. 4, for the linear excitation polarization oriented 90° with respect to the Cartesian coordinate system,
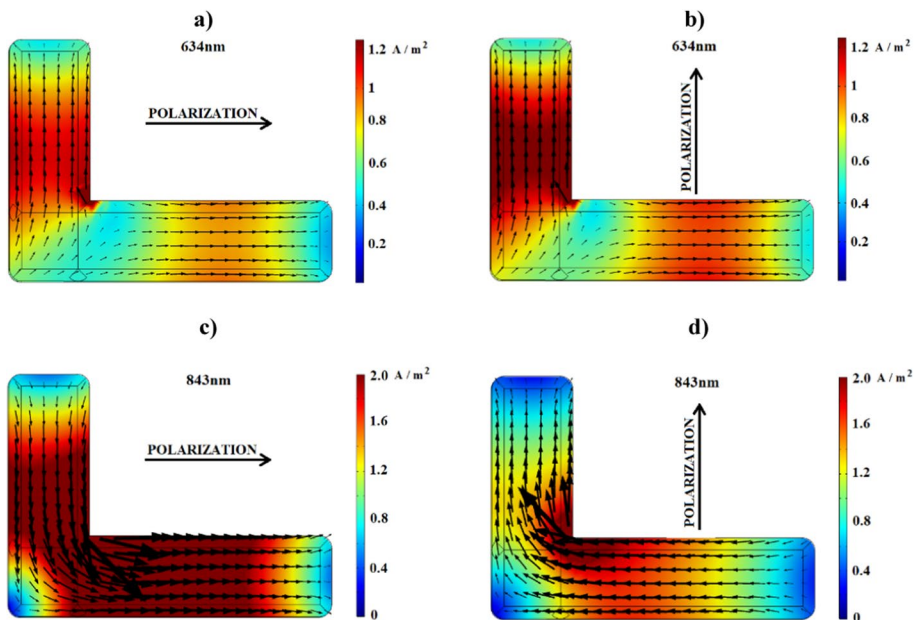

Fig. 3 Current density of the bimodal ROA resonances. Arm lengths are A = 80 nm and B = 60 nm. Color bar is J (current density) with the vector representation of the current modes for ROA configuration from Fig. 1. **a** and **c** ROA resonance wavelengths are 634 nm and 843 nm for polarization direction along x-axis; **b** and **d** ROA resonance wavelengths are 634 nm and 843 nm for polarization direction along x axis
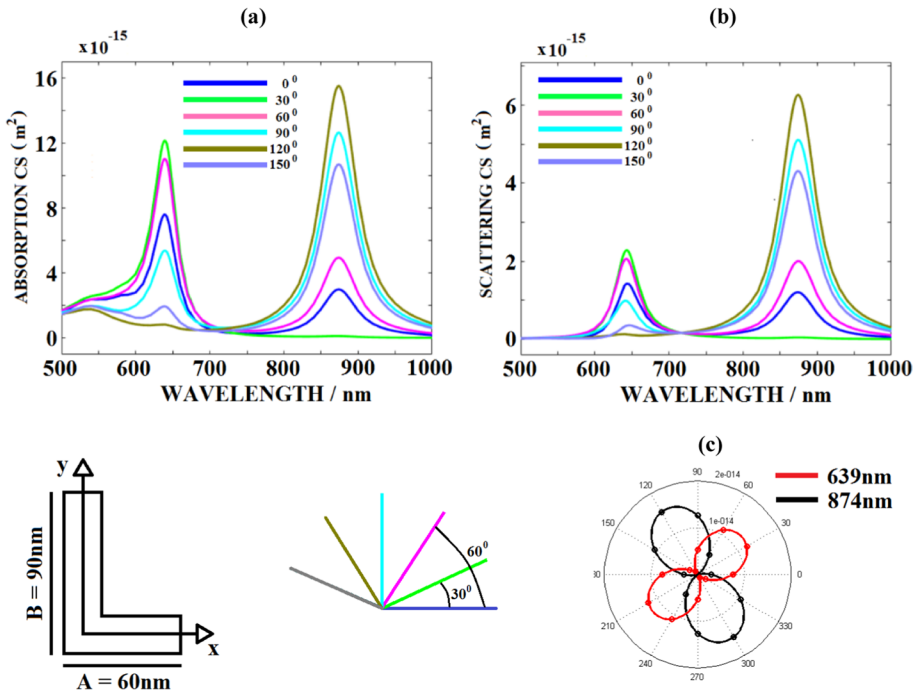
Fig. 4 Electromagnetic plane wave excitation dependence of the scattering and absorption cross section as a function of the polarization angle for an asymmetric L-shaped ROA with arm lengths A = 60 nm and B = 90 nm; **a** absorption cross section with a set of varying linearly polarized plane waves; **b** scattering cross section with a set of varying linearly polarized plane waves; **c** absorption polar diagram of the two asymmetric L-shaped ROA longitudinal resonances for wavelengths 639 nm and 874 nm

both bimodal ROA resonances can be excited. By hitting the internal symmetry main axis of the asymmetric L-shaped ROA as being close to the 30° or 120° (with respect to the x-axis) either the high-frequency ROA mode or the low-frequency ROA mode can be selectively addressed.

Empirically, these specific light polarization states match the effective dipole orientation angles α of the two resonances for the asymmetric L-shaped ROA which can be approximated by the analytical relation:

$$\alpha_{HIGH\_FREQUENCY} = arctg\left[\frac{A - \frac{W}{2}}{B - \frac{W}{2}}\right] \tag{1}$$

and

$$\alpha_{LOW\_FREQUENCY} = \frac{\pi}{2} + arctg\left[\frac{A - \frac{W}{2}}{B - \frac{W}{2}}\right] \tag{2}$$

assuming an analytically single current mode for those resonances. We therefore neglect the influence of the finite width of the ROA arms. These Eqs. (1) and (2) are derived from the geometry sketched in Fig. 5. When the polarization orientation angle is $\alpha_{HIGH\_FREQUENCY}$
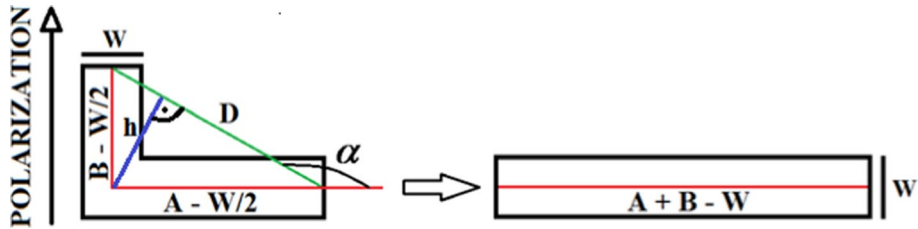
Fig. 5 Representation of the rod-like antenna and L-shaped antenna with the same effective length (or the same volume)

the electric field is polarized along the blue line in Fig. 5 while it is polarized along the green line for a polarization orientation angle $\alpha_{LOW\_FREQUENCY}$.

According to Mie theory, the scattering cross section is a function of the volume of the metallic nanoparticle [30]. It is worth mentioning that we compare spectral properties of single rod-like ROA and L-shaped ROAs which have the same volume. If the width and the height are kept constant (W = 20 nm, H = 30 nm) the same volume could be interpreted as a same effective length of the ROA. As indicated in Fig. 5, for an L-shaped antenna which has antenna arm lengths A and B, an appropriate rod with equal volume has a length $L = A + B — W$. This equation is the result of our approximation that the red line stands for a virtual single electron path for the electrons which travel from end to end of the nanoparticle and represents a longitudinal mode. At the beginning, a rod-like ROA with a length of 100 nm is chosen. The simulation started with a new set of ROAs to investigate the scattering properties for several L-shaped antennas with the same volume. According to the equation $L = A + B — W$ and values L = 100 nm and W = 20 nm, the sum of the L-shaped antennas arm lengths needs to be A + B = 120 nm. For several L-shaped antennas whose arms fulfill this condition, we calculated the scattering responses for the case of polarization in the y-direction. The results in the form of far-field properties are shown in Fig. 6. As

Fig. 6 Far field scattering properties of single L-shaped ROAs with the same effective length and different asymmetries. D is diagonal as shown on Fig. 5
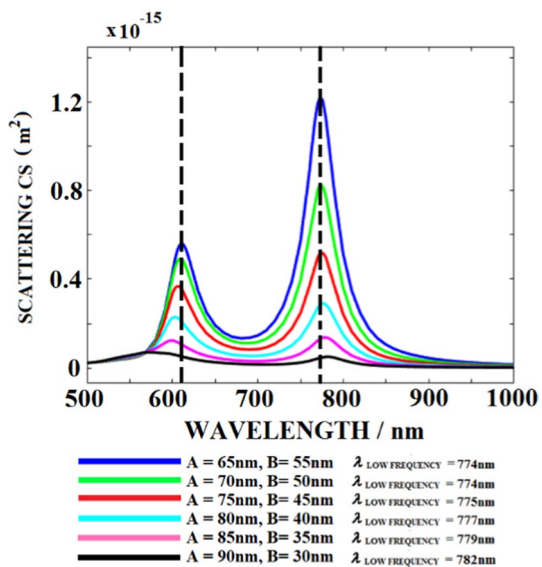
shown in Fig. 6, shortening the length of the arm B and increasing the length of ROA's arm A leads to shifting the high-energy ROA resonance to the high-energy side. On the other hand, we also observe a shift of the low-energy ROA resonance to the low-energy side of the spectral bandwidth (the exact data for D and $\lambda_{LOW\_FREQUENCY}$ are given in Fig. 6 and the behavior of the high-frequency resonant peak wavelength is shown in Fig. 7. This behavior agrees with the general dependence that the blue line gets shorter while the green diagonal line becomes longer when $A + B$ is kept constant while B is reduced.

Analyzing the solutions of the 3D-Maxwell solver in terms of the vector representation of the current flow together with the amplitude of the current modes as depicted in Fig. 3 for the two fundamental ROA resonance frequencies, we deduce that a linear combination of two plasmon length basis functions are sufficient to reconstruct the eigenmodes of the asymmetric L-shaped ROAs. In this sense, a hypothetical hybridization model shall be evaluated, as depicted in Fig. 8. We start with the plasmon length of a short gold nanobar with a dimension of 120 nm. The physical size/dimension of this single gold nanorod represents the base function of the independent plasmon length since the current oscillation at this longitudinal eigenfrequency is confined to the end-to-end phase condition. Nanorods with a length of 120 nm can be bent in the form of an L-shaped nanoparticle with arms 80 nm and 60 nm. This corresponds to the effective length of this L-shaped nanoparticle as it already comprises the additional of the width of 20 nm (80 nm + 60 nm – 20 nm = 120 nm). For the 120 nm gold nanorod ROA with a longitudinal resonance eigenmode energy of 1.44 eV (corresponding to a wavelength of 862 nm) and the 60 nm gold nanorod with the according resonance at 1.88 eV (corresponding to a wavelength of 658 nm). These L-shaped nanostructures have high and low energy resonances at 634 nm and 843 nm with corresponding energies of 1.96 eV and 1.47 eV, respectively. Asymmetric L-shaped ROAs can be constructed to be linear combinations of two resonances. For further analysis is very important to understand Fig. 6 where resonant wavelengths are calculated for different combinations of arm lengths. Therefore, Table 2 discusses the high energy and low energy resonant wavelengths for different combinations of arms A and B of L-shaped ROA, all having the same effective length (A + B-W = 120 nm). Figure 6 shows that while the length of the shorter arm decreases, the high energy resonance is shifting blue. The same behavior can be seen in Table 2, columns 2 and 5. This is in strong correlation with the abovementioned behavior from Fig. 3 where it is pointed out that the highest current density amplitude is exclusively located at the shorter ROA arm of the L-shaped
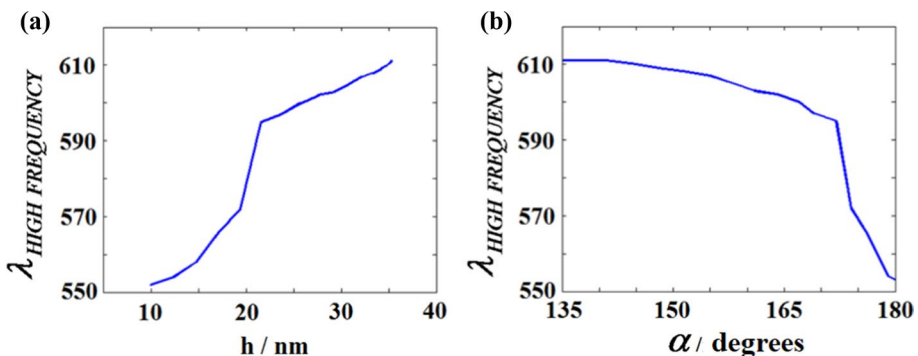

Fig. 7 Relation between high energy mode wavelength and: **a** height of the single L-shaped ROAs (see Fig. 5); **b** angle α of single L-shaped ROAs (see Fig. 5)
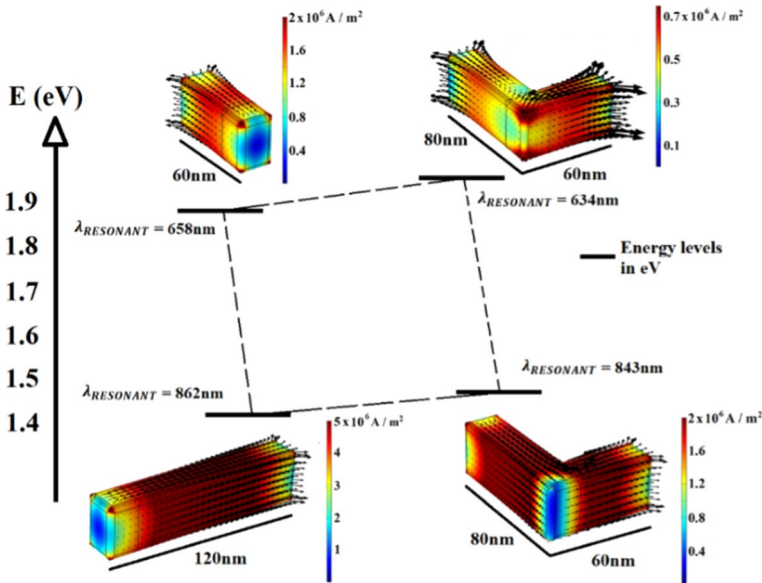
Fig. 8 Energy reconstruction of the asymmetric L-shaped ROA made from single rod-shaped antenna with length 120 nm

antenna giving rise to the high energy resonance. Regarding the low-energy resonance, Table 2 (columns 3 and 6) shows that for a constant effective length of L-shaped antennas (120 nm in this case) and every combination of arms' lengths, the low-energy resonance remains almost stable, except for a small red-shift which is related to the change of the diagonal of the L-shaped nanostructure already analyzed in Figs. 5 and 6. Moreover, it can be seen in Fig. 8 that the plasmon length of the L-shaped ROA defining the low energy eigenmode is shorter than the 120 nm individual gold nanorod, which has the same volume as the given L-shaped ROA. This low-energy ROA resonance does correlate to a plasmon length of 112 nm, which we confirmed via numerical simulations for a single gold nanorod with this particular physical length. But, if A and B are 90 nm and 50 nm, 95 nm and 45 nm, etc., that rule does not apply anymore. Therefore, it is much easier to estimate an L-shaped antenna's low energy resonance position based on the effective length of the L-shaped nanoantenna than to estimate the high energy resonance position. The two fused ROA arms of this eigenmode solution are oscillating out-of-phase along each' individual' arm of the L-shape with a well-pronounced current amplitude located at the short axis of this entity (Figs. 3 and 8). This hybridization picture of plasmon length from individual longitudinal, unperturbed plasmon resonators finds analogies in the field of molecular orbital hybridization of binuclear atomic species A and B, where the hybridization eigenvalues of the symmetric and antisymmetric linear combinations give rise to highly polarized two-center-two-electron covalent bindings. This analogy picture even holds for the symmetric L-shaped ROA (e.g., antenna arm A = 60 nm; B = 60 nm), where the eigenmode energy separation of plasmon length linear combination is symmetrically spread around the plasmon length basis function for the 60 nm gold nanorod (here, 1.88 eV). The design of multiple resonance optical antennas can benefit from the 'fused' plasmon length concept. Thus, broadband ROA devices with well defined tailored resonances can be engineered by tuning the individual plasmon length of each contributing antenna arm.

Table 2 Resonant wavelengths of different L-shaped and rod-shaped structures

1	2	3	4	5	6	7	8
A arm/nm	B arm/nm	Diagonal of the "triangle" (red line in Fig. 5)/nm	Height of the "triangle" (blue line in Fig. 5)/nm	High energy resonant λ of L-shaped antenna with arms A and B/nm	Low energy resonant λ of L-shaped antenna with arms A and B/nm	Resonant λ of nanorod with length B/nm	Resonant λ of nanorod with length 120/nm
70	70	84.9	57.7	634	841	689	862
75	65	85.1	57.3	634	842	672	862
80	60	86	55.8	632	842	657	862
85	55	87.5	53.5	630	843	640	862
90	50	89.4	50.3	628	843	625	862
95	45	91.9	46.5	625	844	611	862
100	40	94.9	42.2	624	846	599	862

Furthermore, the polarization of the re-emitting light can be analyzed in terms of the effective internal dipole of the specific ROA resonance frequency. Therefore, mono-modal ROA resonance scattering and absorption can be accomplished even with a bi-modal asymmetric L-shaped ROA through the polarization control of the external linearly polarized excitation source.
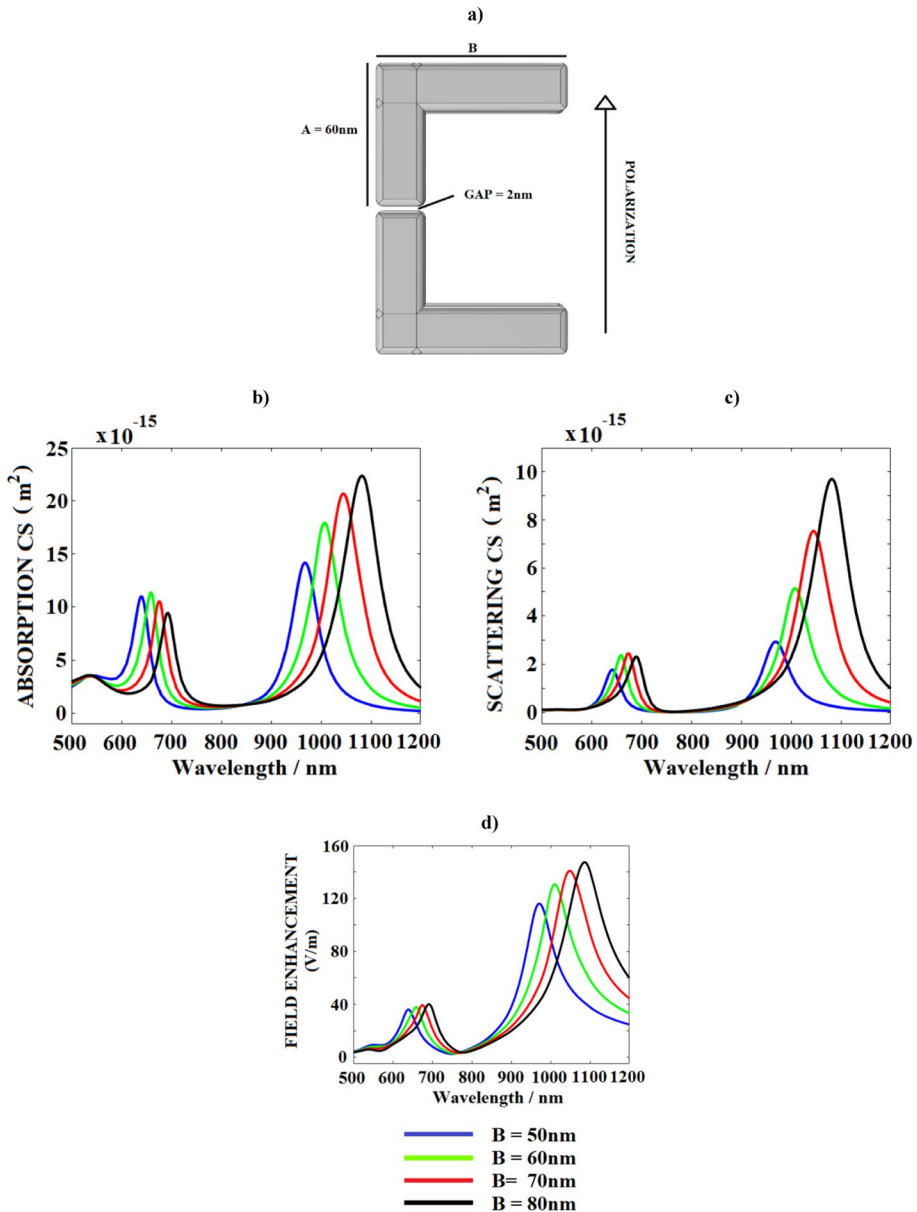
Fig. 9 **a** Top view of a coupled L-shaped ROA (x–y plane) with antenna arms termed A and B where B varies from 50 to 80 nm and A is kept constant at 60 nm; **b** and **c** Absorption and scattering cross section; d) Field enhancement in the gap center at different values of B;

b.   Coupled L-shaped Results

In order to calculate the electric field enhancement, a second L-shaped antenna has been added. Figure 9a shows the top view for the reported coupled L shaped nanoantenna design, while Figs. 9b and c show near and far field properties of coupled L-shaped structures. It can be seen from these Figures that the absorption and scattering cross sections for coupled L-shaped antennas have very similar nature as the single L-shaped antennas shown in Fig. 2. When increasing the arm's length B, there is a red shift of low and high energy resonances and the second resonance amplitude is increased. Figure 9d displays the field enhancement for the coupled L-shaped design.

Here, it is crucial to investigate the behavior for a very small gap of 2 nm width. Regarding near-field behavior, we measure field enhancement in the center of the gap as shown in Fig. 9a. It is worth mentioning that, in this study, the scale for field enhancement here is $|E_{TOT}|/|E_{IN}|$. For the antenna arm lengths A = 60 nm and B = 80 nm, the field enhancements in the gap amount to 40 and 147.3 for the high energy and low energy resonance, respectively. What can be noticed in Fig. 9d is that by increase of arm length B, there is a visible but small red shift of the high energy resonance, but there is no big change of field enhancement. On the other hand, by increasing the length of arm B, there is a significant red shift of the low energy resonance and also a huge increase in field enhancement. We conclude that with the suggested design in Fig. 9a we are able to control field enhancement properties, especially for the low energy resonance.

4 Conclusion

In this paper, a novel design based on L-shaped nano-antennas is proposed and numerically investigated via the finite element method. The reported designs exhibit monomodal and bimodal resonance behavior with a high field enhancement of 40 for high energy and 147.3 for low energy resonance. By changing the length of the antenna, the mode resonances can be tuned. The obtained results and the analysis pave the road for multiple plasmon resonances devices with ultra-high field enhancement that can be integrated with optical nano-circuits with multiple operational frequencies, e.g., frequency conversion devices.

Declarations

References

Bai, Y., Zhao, L., Ju, D., Jiang, Y., Liu, L.: Wide-angle, polarization-independent and dual-band infrared perfect absorber based on L-shaped metamaterial. Opt. Express **23**(7), 8670–8680 (2015). https://doi.org/10.1364/OE.23.008670

Balanis, C.A.: Antenna Theory: Analysis and Design. Wiley, New York (2005)

Bharadwaj, P., Deutsch, B., Novotny, L.: Optical antennas. Adv. Opt. Photonics **1**(3), 438–483 (2009). https://doi.org/10.1364/AOP.1

Biagioni, P., Huang, J.-S., Hecht, B.: Nanoantennas for visible and infrared radiation. Rep. Prog. Phys. **75**(2), 024402 (2012). https://doi.org/10.1088/0034-4885/75/2/024402

Black, L.J., Wiecha, P.R., Wang, Y., Groot, C.H., Paillard, V., Girard, C., Muskens, O.L., Arbouet, A.: Tailoring second-harmonic generation in single L-shaped plasmonic nanoantennas from the capacitive to conductive coupling regime. ACS Photonics **2**(11), 1592–1601 (2015). https://doi.org/10.1021/acsphotonics.5b00358

Bohren, C.F., Huffman, D.R.: Absorption and Scattering of Light by Small Particles. John Wiley & Sons Inc (1983)

COMSOL Multiphysics Software; https://www.comsol.com

Curto, A.G., Volpe, G., Taminiau, T.H., Kreuzer, M.P., Quidant, R., van Hulst, F., Niek.: Unidirectional emission of a quantum dot coupled to a nanoantenna. Science **329**(5994), 930–933 (2010). https://doi.org/10.1126/science.1191922

Dopf, K., Moosmann, C., Kettlitz, S.W., Schwab, P.M., Ilin, K.S., Siegel, M., Lemmer, U., Eilser, H.-J.: Coupled T-shaped optical antennas with two resonances localized in a common nanogap. ACS Photonics **2**(11), 1644–1651 (2015). https://doi.org/10.1021/acsphotonics.5b00446

Feichtner, T.H., Selig, O., Hecht, B.: Plasmonic nanoantenna design and fabrication based on evolutionary optimization. Opt Express **25**(10), 10828–10842 (2017). https://doi.org/10.1364/OE.25.010828

Fromm, D.P., Sundaramurthy, A., Schuck, P.J., Kino, G., Moerner, W.E.: Gap-dependent optical coupling of single "Bowtie" nanoantennas resonant in the visible. Nano Lett. **4**(5), 957–961 (2004). https://doi.org/10.1021/nl049951r

Giannini, V., Fernández-Domínguez, A.I., Heck, S.C., Maier, S.A.: Plasmonic nanoantennas: fundamentals and their use in controlling the radiative properties of nanoemitters. Chem. Rev. **111**(6), 3888–3912 (2011). https://doi.org/10.1021/cr1002672

Jing, Y., Jia-Sen, Z., Xiao-Fe, W., Qi-Huang, G.: Resonant modes of L-shaped gold nanoparticles. Chin. Phys. Lett **26**(6), 067802 (2009). https://doi.org/10.1088/0256-307X/26/6/067802

Johnson, P.B., Christy, R.W.: Optical-constants of noble-metals. Phys. Rev B **6**(12), 4370–4379 (1972). https://doi.org/10.1103/PhysRevB.6.4370

Kelly, K.L., Coronado, E., Zhao, L.L., Schatz, G.C.: The optical properties of metal nanoparticles: the influence of size, shape, and dielectric environment. J. Phys. Chem. B **107**(3), 668–677 (2008). https://doi.org/10.1021/jp026731y

Kern, J., Kullock, R., Prangsma, J., Emmerling, M., Kamp, M., Hecht, B.: Electrically driven optical antennas. Nat. Photonics **9**(9), 582–586 (2015). https://doi.org/10.1038/nphoton.2015.141

Khalil, U.K., Farooq, W., Iqbal, J., Kazmi, S.Z.U.A., Khan, A.D., Rehman, A.U., Ayub, S.: Design and optimization of bowtie nanoantenna for electromagnetic field enhancement. Eur. Phys. J. plus **136**(7), 754 (2021). https://doi.org/10.1140/epjp/s13360-021-01702-7

Kneipp, K., Wang, Y., Kneipp, H., Perelman, L.T., Itzkan, I., Dasari, R.R., Feld, M.S.: Single Molecule Detection Using Surface-Enhanced Raman scattering (SERS). Phys. Rev. Lett. **78**(9), 1667–1670 (1997). https://doi.org/10.1103/PhysRevLett.78.1667

Kosako, T., Kadoya, Y., Hofmann, H.F.: Directional control of light by a nano-optical Yagi-Uda antenna. Nat Photonics **4**(5), 312 (2010). https://doi.org/10.1038/nphoton.2010.34

Li, Z., Hattori, H.T., Parkinson, P., Tian, J., Fu, L., Tan, H.H., Jagadish, C.: A plasmonic staircase nano-antenna device with strong electric field enhancement for surface enhanced Raman scattering

(SERS) applications. J. Phys. D Appl. Phys. **45**(30), 305102 (2012). https://doi.org/10.1088/0022-3727/45/30/305102

Miao, Y., Boutelle, R.C., Blake, A., Chandrasekaran, V., Sheehan, C.J., Hollingsworth, J., Neuhauser, D., Weiss, S.: Super-resolution imaging of plasmonic near-fields: overcoming emitter mislocalizations. J. Phys. Chem. Lett. **13**(20), 4520–4529 (2022). https://doi.org/10.1021/acs.jpclett.1c04123

Mühlschlegel, P., Eisler, H.-J., Martin, O.J.F., Hecht, B., Pohl, D.W.: Resonant optical antennas. Science **308**(5728), 1607–1609 (2005). https://doi.org/10.1126/science.1111886

Novotny, L.: Effective wavelength scaling for optical antennas. Phys. Rev. Lett. **98**(26), 266802 (2007). https://doi.org/10.1103/PhysRevLett.98.266802

Novotny, L., van Hulst, F.N.: Antennas for light. Nat. Photonics **5**(2), 83–90 (2011). https://doi.org/10.1038/nphoton.2010.237

Palomba, S., Novotny, L.: Nonlinear excitation of surface plasmon polaritons by four-wave mixing. Phys. Rev. Lett. **101**(5), 056802 (2008). https://doi.org/10.1103/PhysRevLett.101.056802

Ringe, E., Langille, M.R., Sohn, K., Zhang, J., Huang, J., Mirkin, C.A., Van Duyne, R.P., Marks, L.D.: Plasmon length: a universal parameter to describe size effects in gold nanoparticles. J. Phys. Chem. Lett. **3**(11), 1479–1483 (2012). https://doi.org/10.1021/jz300426p

Schwab, P.M., Moosmann, C., Wissert, M.D., Schmidt, E.W.-G., Ilin, K.S., Siegel, M., Lemmer, U., Eisler, H.-J.: Linear and nonlinear optical characterization of aluminum nanoantennas. Nano Lett. **13**(4), 1535–1540 (2013). https://doi.org/10.1021/nl304692p

Sederberg, S., Elezzabi, A.: Nanoscale plasmonic contour bowtie antenna operating in the mid-infrared. Opt. Express **19**(16), 15532–15537 (2011). https://doi.org/10.1364/OE.19.015532

Seo, E., Choi, B.K., Kim, O.: Particle plasmon resonances in L-shaped gold nanoparticles. Opt. Express **18**(16), 16601–16606 (2010). https://doi.org/10.1364/OE.18.016601

Tahir, A., Schulz, S.A., Leon, I.D., Boyd, R.W.: Design principles for wave plate metasurfaces using plasmonic L-shaped nanoantennas. J. Opt. **19**, 035001 (2017). https://doi.org/10.1088/2040-8986/aa5648

Veselago, V.G.: The electrodynamics of substances with simultaneously negative values of ε and μ. Sov. Phys. Usp. **10**, 509 (1968). https://doi.org/10.1070/PU1968v010n04ABEH003699

Wang, W., Guo, Z., Sun, Y., Shen, F., Li, Y., Lio, Y., Wang, X., Qu, S.: Ultra-thin optical vortex phase plate based on the L-shaped nanoantenna for both linear and circular polarized incidences. Opt. Commun. **355**, 321–325 (2015). https://doi.org/10.1016/j.optcom.2015.06.074

Wissert, M.D., Schell, A.W., Ilin, K.S., Siegel, M., Eisler, H.-J.: Nanoengineering and characterization of gold dipole nanoantennas with enhanced integrated scattering properties. Nanotechnology **20**(42), 425203 (2009). https://doi.org/10.1088/0957-4484/20/42/425203

Xu, Y., Gao, B., He, A., Zhang, T., Zhang, J.: Three-dimensional plasmonic nano-router via optical antennas. Nanophotonics **10**(7), 1931–1939 (2021). https://doi.org/10.1515/nanoph-2021-0094

Yang, J., Zhang, J.: Subwavelength quarter-waveplate composed of l-shaped metal nanoparticles. Plasmonics **6**(2), 251–254 (2011). https://doi.org/10.1007/s11468-010-9196-x

Yang, J., Zhang, J.: Nano-polarization-converter based on magnetic plasmon resonance excitation in and L-shaped slot antenna. Opt. Express **21**(7), 7934–7942 (2013). https://doi.org/10.1364/OE.21.007934

Yang, J., Zhang, J., Wu, X., Gong, Q.: Electric field enhancing properties of the V-shaped optical resonant antennas. Opt. Express **15**(25), 16852–16859 (2007). https://doi.org/10.1364/oe.15.016852

Yue, W., Wang, Z., Whittaker, J., Lopez-royo, F., Yang, Y., Zayats, A.V.: Amplification of surface-enhanced Raman scattering due to substrate-mediated localized surface plasmons in gold nanodimers. J. Mater. Chem. C **5**(16), 4075–4084 (2017). https://doi.org/10.1039/C7TC00667E

Zienkiewicz, O.C., Taylor, R.L., Zhu, J.Z.: Finite element method: its basis and fundamentals. Butterworth Heinemann, London (2005)